Received: 24 February 2023 | Revised: 15 May 2023 | Accepted: 20 May 2023

DOI: 10.1111/cas.15878

ORIGINAL ARTICLE

Cancer Science WILEY

# Translational screening platform to evaluate chemotherapy in combination with focal therapy for retinoblastoma

Irina L. Sinenko[1,2] | Fabien Kuttler[3] | Valentin Simeonov[4] | Alexandre Moulin[2] | Patrick Aouad[2] | Christina Stathopoulos[2] | Francis L. Munier[2] | Adeline Berger[2] | Paul J. Dyson[1]

[1]Institute of Chemical Sciences and Engineering, École Polytechnique Fédérale de Lausanne (EPFL), Lausanne, Switzerland

[2]Ophthalmology Department, University of Lausanne, Jules-Gonin Eye Hospital, Fondation Asile des Aveugles, Lausanne, Switzerland

[3]Biomolecular Screening Facility, School of Life Sciences, École Polytechnique Fédérale de Lausanne (EPFL), Lausanne, Switzerland

[4]Laboratory of Environmental Remote Sensing, École Polytechnique Fédérale de Lausanne (EPFL), Lausanne, Switzerland

**Correspondence**
Adeline Berger, Ophthalmology Department, Jules-Gonin Eye Hospital, Fondation Asile des Aveugles, University of Lausanne, Avenue de France 15, CH-1004 Lausanne, Switzerland.
Email: adeline.berger@fa2.ch

Paul J. Dyson, Institute of Chemical Sciences and Engineering, École Polytechnique Fédérale de Lausanne (EPFL), Avenue F.-A. Forel 2, CH-1015 Lausanne, Switzerland.
Email: paul.dyson@epfl.ch

**Funding information**
H2020 Marie Skłodowska-Curie Actions, Grant/Award Number: 754354

## Abstract

Retinoblastoma is the most common pediatric eye cancer. It is currently treated with a limited number of drugs, adapted from other pediatric cancer treatments. Drug toxicity and relapse of the disease warrant new therapeutic strategies for these young patients. In this study, we developed a robust tumoroid-based platform to test chemotherapeutic agents in combination with focal therapy (thermotherapy) – a treatment option widely used in clinical practice – in accordance with clinically relevant trial protocols. The model consists of matrix-embedded tumoroids that retain retinoblastoma features and respond to repeated chemotherapeutic drug exposure similarly to advanced clinical cases. Moreover, the screening platform includes a diode laser (810 nm, 0.3 W) to selectively heat the tumoroids, combined with an on-line system to monitor the intratumoral and surrounding temperatures. This allows the reproduction of the clinical settings of thermotherapy and combined chemothermotherapy treatments. When testing the two main drugs currently used in clinics to treat retinoblastoma in our model, we observed results similar to those clinically obtained, validating the utility of the model. This screening platform is the first system to accurately reproduce clinically relevant treatment methods and should lead to the identification of more efficient drugs to treat retinoblastoma.

**KEYWORDS**
cancer chemotherapy protocol, chemotherapy, chemothermotherapy, preclinical model, retinoblastoma, thermotherapy

**Abbreviations:** EGF, epidermal growth factor; FFPE, formalin-fixed-paraffin-embedded; FGF, fibroblast growth factor; GEMM, genetically-engineered mouse model; HA, hyaluronic acid; ICG, indocyanine green; LIF, leukemia inhibitory factor; PDX, patient-derived xenograft; *RB1*, retinoblastoma gene; TER, thermal enhancement ratio.

## 1 | INTRODUCTION

Retinoblastoma is the most common intraocular malignancy of childhood that is typically diagnosed in infants under the age of 5 years.[1] While the survival rate in high-income countries is higher than 95%, the relapse rate, incidence of secondary tumors, and side-effects associated with treatments remain a challenge.[2,3] Retinoblastoma originates from cone-precursors.[4] While growing, tumor cells can detach from the primary intraretinal mass and seed into various nonvascularized eye compartments such as the vitreous and the subretinal space or the aqueous humor.[5,6] Chemotherapy, under different injection routes, is broadly used to treat retinoblastoma at each stage.[7] Intravenous and intra-arterial chemotherapy are typically used as a first-line or salvage treatment for retinal and subretinal disease, while intraocular injections are necessary to manage intravitreal and/or aqueous seeding.[8–10] Thermotherapy can be used isolated for small retinal or subretinal tumor or tumor relapses or combined with systemic chemotherapy (chemothermotherapy).[11–13]

Systemic chemotherapeutic agents currently used to treat retinoblastoma, such as carboplatin, etoposide, and vincristine, were not specifically developed for this disease or identified through a systematic screening approach, but rather chosen through pilot studies based on their performance in other pediatric cancers.[14] In contrast, melphalan was found to be the most tumoricidal drug among 12 other drugs in vitro and is used exclusively for targeted chemotherapy (intra-arterial or intraocular injections) due to its high systemic toxicity.[15] To date, there are no common standardized protocols concerning the treatment regimen (drug type or drug combination) among the centers. Treatment resistance and/or tumor progression despite therapy are managed with enucleation to avoid tumor spread. Finally, cases with extraocular spread at diagnosis or during conservative management, especially those with central nervous involvement, are associated with a poor survival outcome due to the insufficient efficacy of the current available chemotherapy drugs. Preclinical models that mimic the clinical methods should facilitate the discovery of new drugs to overcome the above-mentioned limitations.

Preclinical retinoblastoma models include cellular models and animal models (both transgenic and xenograft).[16–19] While in vivo transgenic animal models, that is, GEMMs, are able to depict some tumorigenic aspects of the disease, there are genomic and epigenomic differences between mice and humans.[21] Particularly in the case of retinoblastoma, as the cell of origin is different in these two species, mice are not an optimal organism to study this specific disease. Xenograft models, or PDX, resemble growth patterns of patient retinoblastoma, but species specificities of the microenvironment could result in genetic heterogeneity and induce major changes within the tumor cells.[22] Regarding treatment development, the choice of in vivo model significantly impacts on the response of the tested drug. For instance, a comparative study of a systemic chemotherapy protocol in both GEMMs and PDX models revealed a complete and a poor response, respectively.[23] In contrast, in vitro cellular models present certain advantages, such as ease of maintenance and growth, accessibility, and facile imaging. Nevertheless, most conventional in vitro models lack organization and cell–cell and cell-matrix interactions, factors that impact strongly on drug performance.[24]

An alternative to preclinical models comprises 3D in vitro cultures or tumoroids, which overcome cross-species alterations (as seen in the animal models) and lack of complexity (as seen in cellular models). These 3D models provide important insights into the biology and tumorigenesis and are able to reflect parental tumor features,[25–27] which make them an advanced in vitro filter for prospective drug candidate screening. Although retinoblastoma tumoroids have been reported previously,[27] they have not been adapted to the diversity of therapeutic approaches used to treat retinoblastoma, and hence there is currently an unmet need in adapted models to investigate new drug candidates or drug combinations in various and adjustable clinically relevant settings.

In this study, we present a robust 3D tumoroid system used to validate clinically relevant chemotherapy and chemothermotherapy protocols, mimicking treatments currently used for the solid and liquid forms of retinoblastoma tumors. The system allows drug screening alone or in combination with thermotherapy, facilitating the discovery of treatment candidates for retinoblastoma.

## 2 | MATERIALS AND METHODS

### 2.1 | Cell culture

Human retinoblastoma cell lines Y79 and WERI-Rb1 were cultured according to the manufacturer instructions (identifier and source of all materials used in this study are summarized in Table S1).

### 2.2 | Free-floating spheroids

To define optimal conditions for 3D culture, cells were grown under 12 different conditions described in the manuscript. The different base media used consist of DMEM:F-12, RPMI-1640, or neurobasal medium. Media were supplemented with either 20% FBS or 20 ng/mL recombinant human EGF, 20 ng/mL recombinant human basic FGF, 20 ng/mL recombinant human LIF, 1× B27 supplement minus vitamin A, 100 IU/mL penicillin–streptomycin, and 5 μg/mL heparin. Additionally, cells were cultured either in the presence or absence of 100 g/mL HA at the same concentration endogenously found in human vitreous.[28,29]

### 2.3 | Basement membrane matrix-embedded tumoroids

Tumoroids were generated as described previously with protocol modifications.[27] In brief, single cell suspension was embedded in growth factor reduced Matrigel (Corning), Geltrex (ThermoFisher), or Cultrex Type 2 (Bio-Techne) to the final protein concentration of

6 mg/mL, 10 mg/mL, and 6 mg/mL, respectively. Cell density was adjusted to $5.0 \times 10^4$ cells/mL to avoid over-confluency by the endpoint of tumoroid generation (3 weeks). Drops (20 μL) were polymerized at 37°C and overlaid with prewarmed culture medium (complete RPMI-1640 medium supplemented with either 20% FBS for Y79 tumoroids, or 10% FBS for WERI-Rb1 tumoroids) and maintained in a humidified incubator under 5% $CO_2$ at 37°C, with medium changed twice a week. Tumoroids were grown for 3 weeks and then assessed for further experiments.

## 2.4 | Immunohistochemistry

Tumoroids were extracted from the matrix with Cell Recovery Solution (Corning), fixed in 4% MeOH-free formaldehyde, then embedded in HistoGel (Epredia) and later in paraffin.

Immunohistochemistry and immunofluorescence were carried out on a series of either 6 μm-thick cryosections or on 4 μm FFPE sections. Antigen retrieval in citrate buffer at pH 6 was done prior to blocking for FFPE sections. Slides were blocked for 1 h with 10% normal goat serum, incubated overnight with the primary Ab diluted in blocking buffer, and washed three times with PBS. Slides were incubated with appropriate secondary Ab for 1 h, washed three times with PBS, and counterstained with DAPI and/or rhodamine phalloidin. Antibodies used in this study are summarized in Table S1.

## 2.5 | Quantitative RT-PCR

Tumoroids were extracted from the matrix with Cell Recovery Solution (Corning), and total RNA was isolated with an RNeasy Mini Kit (Qiagen). A NanoDrop 2000C spectrophotometer (Thermo Scientific) was used to quantify the isolated RNA. Subsequently, a High-Capacity cDNA Reverse Transcription Kit (Applied Biosystems) was used to reverse transcribe the total RNA into cDNA. Quantitative RT-PCR was undertaken using FastStart Essential DNA Green Master (Roche). Primers for human genes were designed with the Primer-BLAST tool (NCBI NLM NIH) and synthesized by Merck. The primer sequencings are summarized in Table S2. *ATP5B* and *GPI* were used as housekeeping genes.

## 2.6 | Drug screening

### 2.6.1 | PrestoBlue cell viability assay

Drug stock solutions were prepared freshly in DMSO. Cells were plated in 96-well flat-bottom plates at a final concentration of $4 \times 10^5$ cells/mL and then treated. We used DMSO and gambogic acid as negative and positive controls, respectively. Cultures were incubated for 72 h in a humidified incubator under 5% $CO_2$ at 37°C (or, alternatively, for 1 h at 42°C and then transferred to 37°C for 71 h). PrestoBlue (Invitrogen) cell viability reagent was added to cultures at 1:10 ratio, and samples were incubated for 1 h. Fluorescence at 560/590 nm was detected with a SpectraMax M5e microplate reader (Molecular Devices).

### 2.6.2 | Calcein AM–ethidium homodimer-1 cell viability assay

Fresh drug solutions were prepared before usage. Three-weeks postseeding BME-embedded tumoroids were used for the experiment. Samples were treated for 72 h, rinsed with PBS, and labeled with calcein AM and ethidium homodimer-1 according to the manufacturer's protocol (ThermoFisher). Fluorescence imaging and bright field imaging were undertaken with the IN Cell Analyzer 2200 system (GE Healthcare). Automated acquisition was carried out in an environmental chamber (at 37°C with 5% $CO_2$) using a 4×/0.2 NA objective.

## 2.7 | Thermotherapy assessment

The laser illumination system was composed of a laser, imaging optics, and a bending mirror. The laser is a continuous wave, 810 nm semiconductor device. The output power can be controlled manually from 0.1 to 1.0 W. The laser was coupled to a 200 μm optical fiber, which delivers the light to the imaging optics. The imaging optics uses a single aspheric lens to image the end of the optical fiber on the biological sample. The image size on the sample is measured to be 350 μm. Because of the limited space between the microscope condenser unit and the sample stage, a bending mirror was used to deliver the light from the imaging optics to the sample.

Temperature measurements were carried out using a ONE Pro (FLIR), mid infrared camera. The light from the sample to the camera was delivered by a protected silver bending mirror.

To characterize ICG, attenuated transmitted reflectance Fourier transform infrared spectrum was acquired on a Perkin Elmer Spectrum-Two instrument equipped with diamond-anvil configuration; UV/visible/near infrared spectrum was recorded on a Perkin Elmer Lambda 950S spectrometer using quartz cuvettes.

## 2.8 | Data analysis

Image analysis was carried out using CellProfiler 4.2.1 complemented with the module for the deep learning-based segmentation algorithm Cellpose[30] and Fiji ImageJ 1.53q software.

## 2.9 | Statistical analysis

Statistical analyses were undertaken using GraphPad Prism 9.4.0. software. Two-tailed nonparametric tests were used, unless otherwise specified. Significance levels of $^*p \le 0.05$, $^{**}p \le 0.01$, $^{***}p \le 0.001$,

****$p \leq 0.0001$, and not significant ($p \geq 0.05$) were used. Data represent mean ± SD, unless otherwise specified.

## 3 | RESULTS

### 3.1 | Optimization of retinoblastoma tumoroid culture conditions

To determine the experimental settings that allow the growth of retinoblastoma free-floating spheroids, we first defined the optimal culture conditions, based on previously described patient-derived 3D structures.[26,31,32] To better mimic the tumor environment and the contact with the vitreous, that is, to ensure relevant viscosity, HA was added to the media. Dense bulky structures forming spheroids in 3–4 days of culture were obtained from the Y79 cell line under serum-free advanced DMEM/F-12 base medium supplemented with a cocktail of growth factors (EGF, FGF, and LIF), heparin, B-27, and HA (Figure S1). These spheroids were used to evaluate the cytotoxic effect of current retinoblastoma chemotherapeutics, that is, carboplatin, melphalan, etoposide, and topotecan, in dose–response manner. The $IC_{50}$ values did not reveal a significant difference compared to standard 2D suspension culture (Table S3), presumably because the Y79 cell line spontaneously grows as aggregates in suspension (although these aggregates are easily disrupted and not very dense, unlike spheroids). With continuous culture under these conditions, the spheroids tended to show a decreased proliferation rate and viability after approximately 3 weeks.

As the primary retinoblastoma tumor localizes within the neuronal layers of the retina, we hypothesized that the tumor cells will better maintain their properties within a matrix, and consequently implemented a scaffold-based approach into the tumoroid model (a schematic representation of the entire process is shown in Figure 1A). The formation of dense tumoroids was observed 3–4 weeks postseeding from both Y79 and WERI-Rb1 cell lines (Figures 1B and S2A). Various commercially available matrixes were tested (Matrigel, Geltrex, and Cultrex) and all supported tumoroid formation and growth (Figures 1C and S2B). The number and size of the Y79 tumoroids varied in Cultrex matrix compared to the other matrixes (average number of 8 tumoroids in Cultrex vs. 72 and 39 in Matrigel and Geltrex, respectively, at 21 days postseeding; Figure S3), and thus was excluded. Matrigel and Geltrex growth curves both fitted the same equation of exponential growth ($p = 0.6505$). For WERI-Rb1 tumoroids, all matrixes worked similarly. For clarity, Y79 Geltrex-embedded and WERI-Rb1 Cultrex-embedded tumoroids will be described from now on. Three weeks of growth, followed by automated segmentation and quantification of tumoroids in each well, and further two-way ANOVA statistical analysis did not reveal significant intraplate variability (Figures 1D,E and S2C). Nevertheless, variability between some independent experiments (e.g., E9 and E18) was observed, which is probably due to cell variability (Table S4). An increase in tumoroid size, although not significant, correlates with a decreased number of tumoroids per well (Pearson's correlation coefficient, −0.5030; $p = 0.0720$) (e.g., 89 ± 11 tumoroids with a diameter of 156 ± 35 μm [E9] and 34 ± 3 tumoroids with a diameter of 207 ± 50 μm [E36]; Figure 1F). Despite this variability, comparison of dose–response curves from independent experiments did not reveal variation of $IC_{50}$ values ($p = 0.7525$), which makes the tumoroid model suitable and reliable for drug screening and comparison of experiments. Tumoroids in these conditions were alive and proliferative for up to 8 weeks postseeding, which, unlike most of the existing models, allows the implementation of various drug testing protocols (see below).

### 3.2 | Molecular characterization of retinoblastoma tumoroid model

To validate that the integrity of the retinoblastoma cells was conserved when cultured in 3D, structural features and expression of specific markers were investigated at the RNA and protein levels. In 2D and 3D cultures, the morphological features of the Y79 and WERI-Rb1 cells were similar with enlarged, irregular, angulated nuclei with a heterogenous chromatin and scant cytoplasm. In Y79 tumoroids, necrotic cells at the centers of the tumoroids surrounded by a rim of live cells could be identified, as observed clinically and histopathologically in vitreous spheres.[5] Immunohistochemical analysis indicated that both retinoblastoma tumoroids retained the loss of retinoblastoma protein expression with a preserved expression of synaptophysin (Figures 2 and S4). As expected, the proliferative activity (Ki-67) was high, notably in the outer proliferative rim for Y79 tumoroids.[33] Furthermore, the retinoblastoma tumoroids maintained both nuclear expression of early photoreceptor/cone marker orthodenticle homeobox 2 (OTX1-2) and cytoplasmic expression of late cone marker arrestin 3 (ARR3), which would define Y79 and WERI-Rb1 2D and 3D as subtype 2 retinoblastoma, following the classification of Liu et al.[34]

The Y79 tumoroids did not show significant differences in marker gene expression compared to 2D culture when analyzed at the RNA level (Figure S5). The only noticeable difference, although not significant, is a tendency to upregulate the pro-apoptotic factor *BNIP3*, linked to hypoxia, which might indicate the presence of a hypoxic region in the tumoroid model.

### 3.3 | Retinoblastoma tumoroid model as a chemotherapy drug screening platform

Our tumoroid model was initially used to evaluate the chemotherapeutic treatments melphalan and carboplatin, applied as single agents in the clinic to treat liquid or solid intravitreal retinoblastoma tumors. The first treatment protocol implemented (Protocol 1) consisted of 3-week tumoroid generation, followed by 3-day drug exposure ending with a live-dead viability assay using high-throughput imaging and automated high-content analyses (Figure 3A,B). Assay performance was validated as a model for screening with Z'-factor

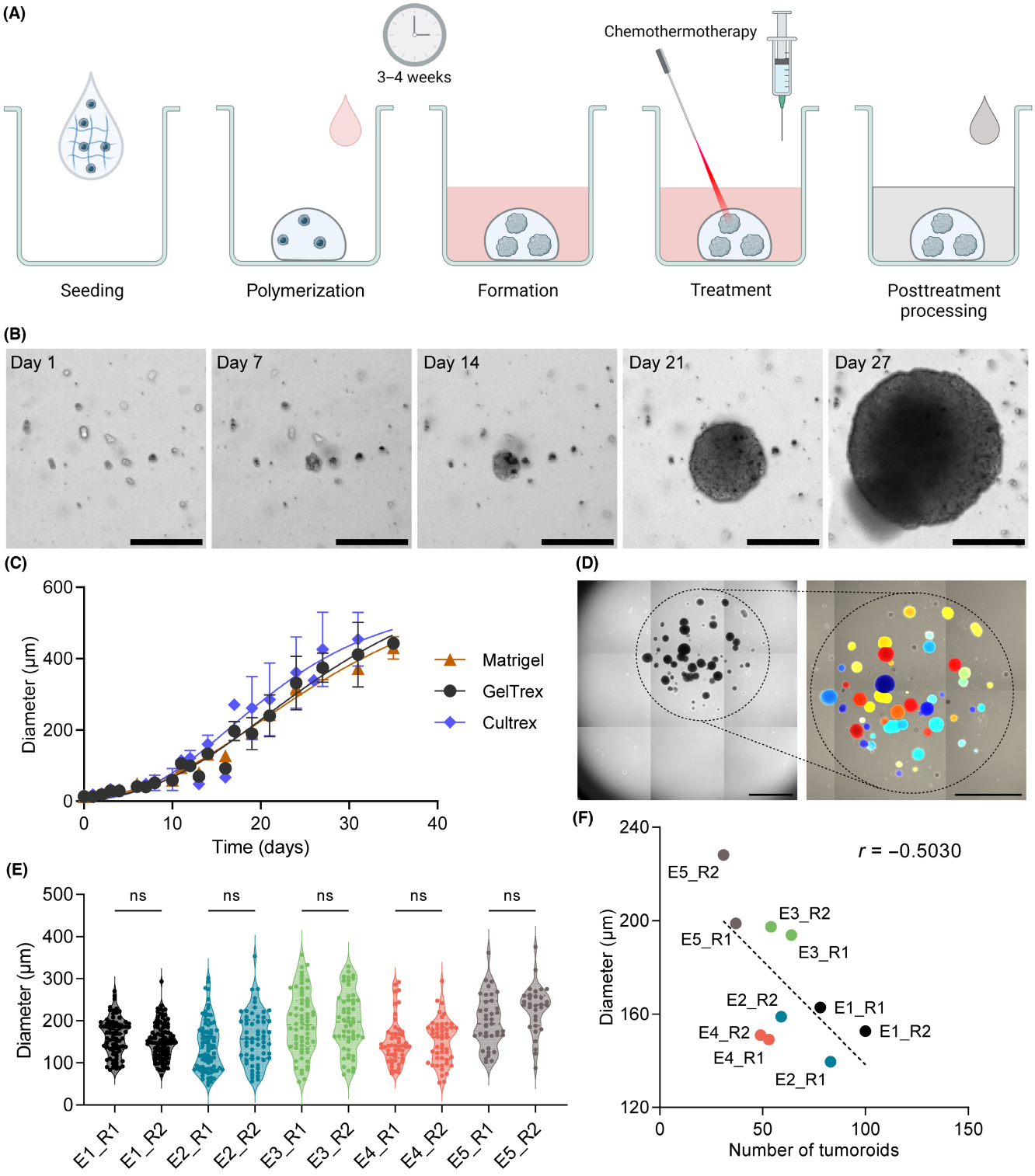


FIGURE 1 Generation of scaffold-based retinoblastoma tumoroids from Y79 cell line. (A) Schematic of tumoroids grown from a single cell in a drop of matrix. (B) Real-time brightfield microscopy images displaying the same single tumoroid grown in Geltrex at different time points. Scale bars, 200 µm. (C) Time course quantification of the size of tumoroids grown in various BME, averaged from three independent experiments. (D) Snapshot of a single well with tumoroids at 21 days postseeding; nine fields of view acquired and brought together allow the full area of the matrix drop in each well to be visualized and analyzed. Dashed circle shows the limit of the matrix drop; colored circles represent mask for further quantification as determined using CellProfiler software complemented with the module for the segmentation algorithm Cellpose. One representative experiment. Scale bars, 2 mm. (E) Diameter variability of tumoroids at 21 days postseeding among independent experiments. Two technical replicates representing one well each are shown per experiment; Kruskal-Wallis statistical test. Dashed line indicates the median, dotted lines indicate the lower and upper quartiles. (F) Correlation of diameter and number of tumoroids at 21 days postseeding among technical replicates (indicated as _R1 or _R2) and independent experiments (E# and color coded). ns, not significant ($p \geq 0.05$).

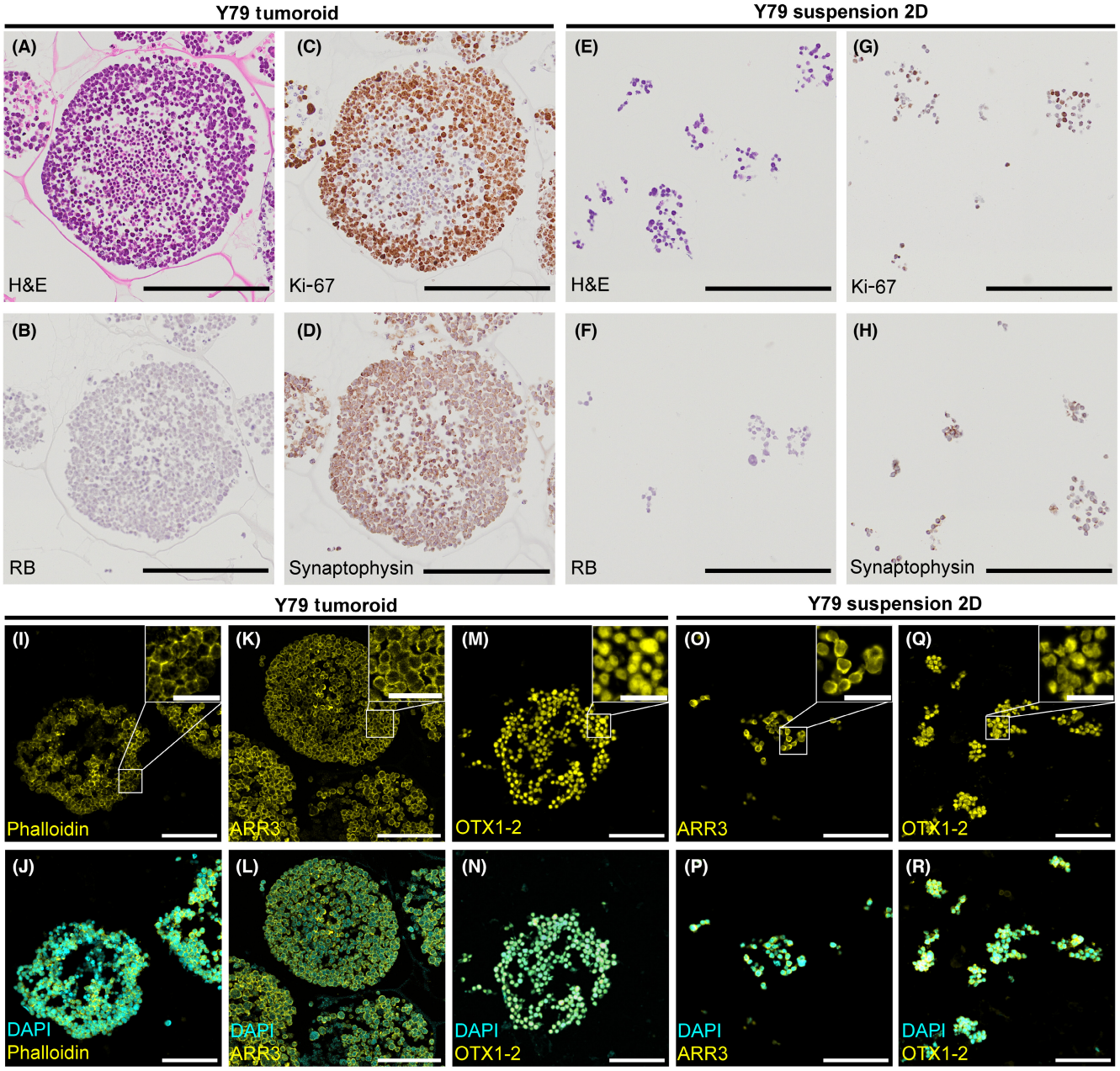


**FIGURE 2** Morphology and molecular features of Y79 retinoblastoma tumoroid model. (A–H) H&E staining, retinoblastoma protein (RB), synaptophysin (SYP), and proliferation marker Ki-67 immunohistochemistry of retinoblastoma tumoroids compared to 2D suspension culture. Scale bars, 200 μm. Staining was carried out on successive sections of the same tumoroid, hence the difference in size of the stained material. (I–R) Immunostaining of phalloidin, arrestin 3 (ARR3), and orthodenticle homeobox 2 (OTX1-2), counterstained with DAPI. Scale bars: panels, 100 μm; insets, 30 μm.

based on fluorescence intensity values of negative (DMSO) and positive (gambogic acid) controls – Z' values above 0.4 were accepted (Figure 3C).[35] The responses of melphalan and carboplatin were investigated and compared to 2D suspension culture. The $IC_{50}$ value of melphalan in Y79 tumoroids was 163 ± 31 μM versus 3.4 ± 0.9 μM in the 2D counterpart (Figure 3D). The $IC_{50}$ values of carboplatin were 843 ± 75 μM and 62 ± 4 μM in tumoroid and 2D culture, respectively (Figure 3D). In WERI-Rb1 tumoroids, $IC_{50}$ values of melphalan were 390 ± 169 μM and 7.5 ± 6.0 μM in 2D; $IC_{50}$ values of carboplatin were 345 ± 77 μM (tumoroid) and 22.6 ± 6.0 μM (2D) (Figure S6, Table S5). This difference is consistent with previous studies showing lower drug sensitivity of 3D structures compared to their 2D counterparts.[36,37] To investigate whether matrix components influence drug efficacy, we studied drug response in the presence of 2% matrix suspension. None of the matrixes tested hindered the efficacy of carboplatin or melphalan (Figure S7). In comparison to the clinically applied doses, reported melphalan dose for intravitreal chemotherapy single injection is 20–40 μg, which corresponds to an intravitreal concentration of 16.5–33 μM.[38] Systemically administered carboplatin at a dose of 560 mg/m$^2$ was

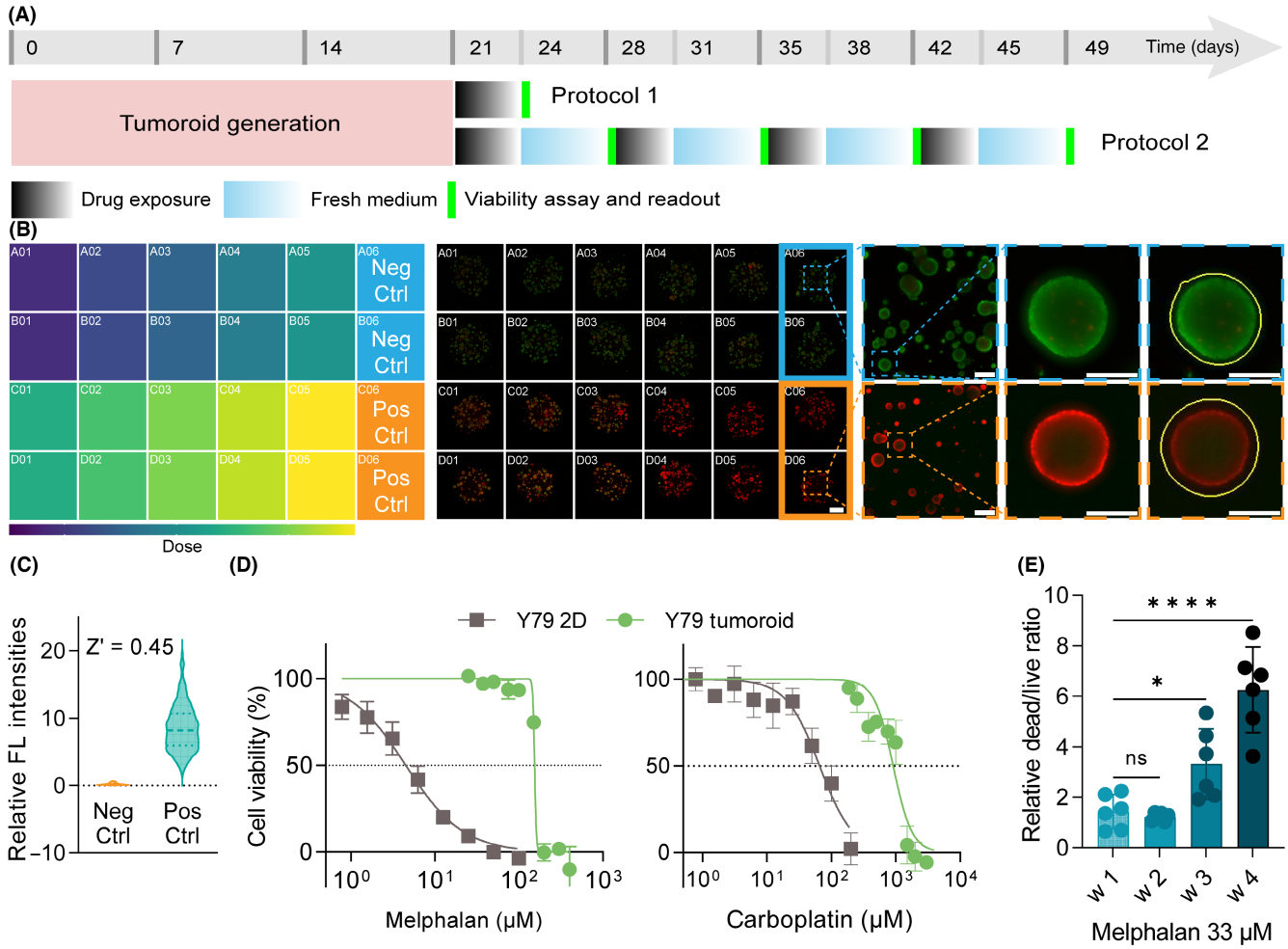


FIGURE 3 Phenotypic drug screening. (A) Timeline of two screening protocols: standard assessment of cytotoxicity (Protocol 1) and a clinically relevant repeated-treatment protocol (Protocol 2). (B) Tiled fluorescence microscopy images of a dose–response experiment on a 24-well plate. Tumoroids were fluorescently labeled with calcein-AM (live, green) and ethidium homodimer-1 (dead, red). As representative examples, the positive control gambogic acid (Pos Ctrl) and the negative control DMSO (Neg Ctrl) were chosen to demonstrate the imaging pipeline. The last column shows the corresponding outlines of objects segmented during image analysis for the selected microscopy images. Scale bars: well plate, 2 mm; well inset, 500 μm; single tumoroids, 200 μm. (C) Violin plots showing the comparison of the relative fluorescence intensity average values (ratio of dead and live channels) and their variability between both positive and negative controls. Dashed line indicates the median, dotted lines indicate the lower and upper quartiles. (D) Dose–response curves of melphalan (left panel) and carboplatin (right panel) on tumoroid model and suspension culture. (E) Repeated treatment protocol with melphalan over 4 weeks of treatment (w 1–w 4); ordinary one-way ANOVA statistical test. *$p \le 0.05$, ****$p \le 0.0001$, ns, not significant ($p \ge 0.05$).

reported to correspond to an intravitreal concentration of 4.05 μg/mL (or 10.91 μM) in enucleated eyes.[39]

To achieve cancer remission, the majority of patients with vitreous liquid seeds need to be exposed to one or several cycles of 2–4-weekly intravitreal injections of melphalan. Hence, to better mimic clinical protocols, tumoroids were exposed to melphalan for four cycles of treatment, each consisting of 3 days of drug exposure followed by medium renewal for 4 days (Protocol 2; Figure 3A). Note that medium renewal was used to adapt the protocol from intravitreal injection to in vitro use, mimicking constant renewal of the vitreous humor and a subsequent decrease of drug amount in the vitreous.[40] Tumoroid viability and size progressively decreased over 4 weeks of treatment (Figures 3E and S8), reflective of clinical observations.[3,38]

### 3.4 | Chemothermotherapy screening – combining tumoroid model with focal therapy

As retinoblastoma primary tumors start from a solid intraretinal growth, chemotherapy is often clinically used in combination with focal thermotherapy. Clinical chemothermotherapy protocols consist of systemic carboplatin treatment followed by laser irradiation for a duration of several minutes, typically 1–16 min.[12,41] In contrast, studies investigating drug candidates for their synergy with heat reproduce hyperthermia conditions in vitro by incubating treated cells at stable elevated temperatures for typically 1–2 h.[42,43] To better mimic clinical conditions, an 810 nm diode laser beam (the same laser type as that used in the clinic) was focused on the tumoroid sample through imaging optics and bending mirrors (Figure 4A). The

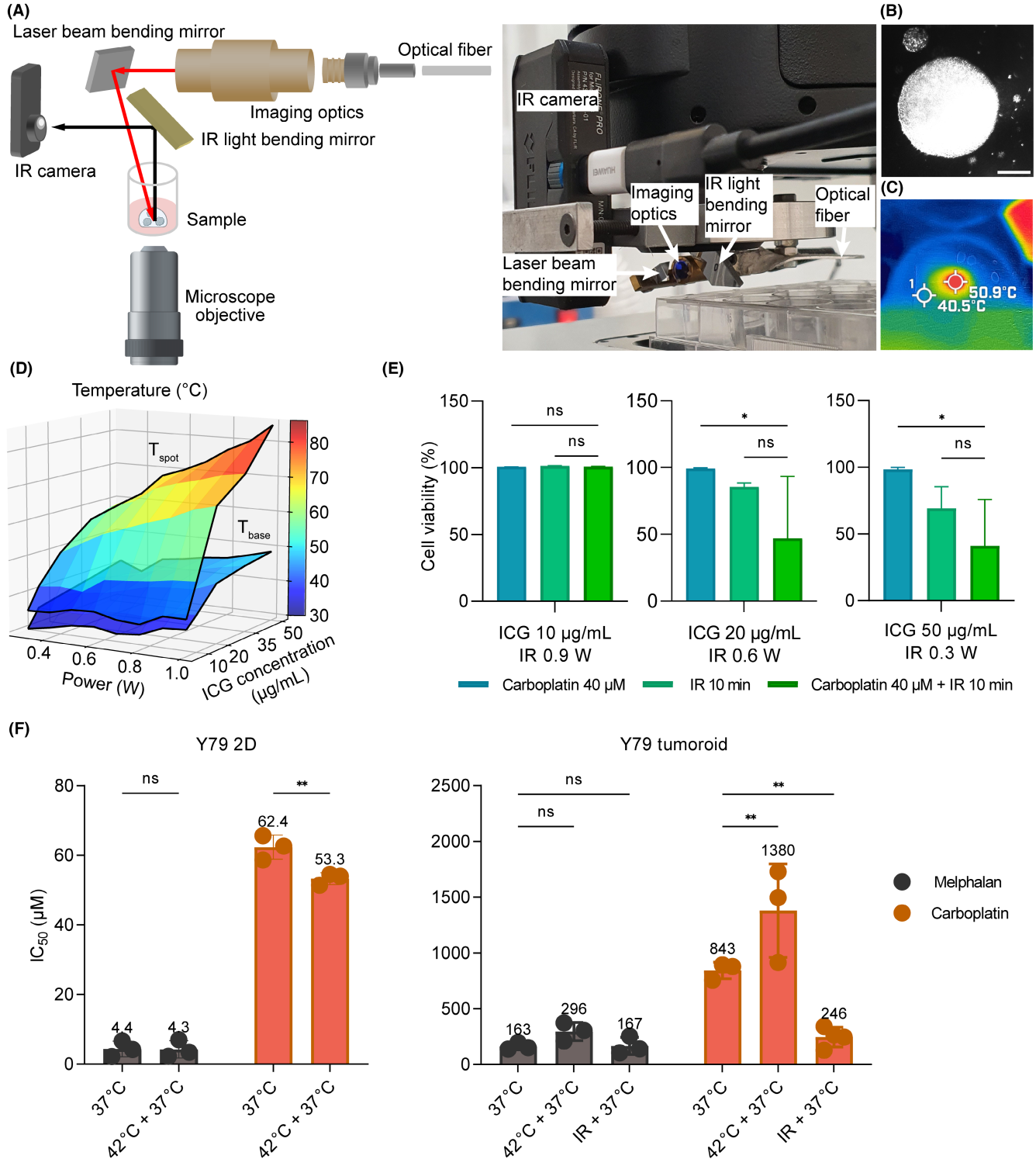


FIGURE 4 Development and optimization of the system for evaluating chemothermotherapy in tumoroids. (A) Schematic and photograph of the illumination system. Red arrows indicate the laser beam path; black arrows indicate the light path to the thermal camera. (B) Real-time brightfield image of the laser beam focused on tumoroid culture. Scale bar, 200 μm. (C) Combined multispectral dynamic image of the laser beam focused in the well. (D) Heatmaps of the laser spot ($T_{spot}$) and base well ($T_{base}$) temperatures. (E) Cytotoxicity of chemo-, thermo-, or combined therapy depending on the concentration of indocyanine green (ICG) and power of the laser. Kruskal–Wallis statistical test. (F) $IC_{50}$ values of carboplatin and melphalan alone or in combination with thermotherapy. Left panel, suspension culture; right panel, tumoroid (comparison of different thermotherapy settings). Ordinary two-way ANOVA statistical test. *$p \le 0.05$, **$p \le 0.01$, ns, not significant ($p \ge 0.05$). IR, infrared.

system was combined with an inverted microscope to enable precise focusing in real-time (Figure 4B). As all the components must fit between the sample stage and the microscope condenser, tumoroids were plated in 24-well plates (the deepness of wells in 48- or 96-wells did not allow the laser beam to be directed on the tumoroid sample due to the limited space between the optics and the plate). A thermal camera was used to monitor and control the temperature of the sample during the procedure (Figure 4C).

Retinoblastoma cells are characteristically not pigmented, which results in low heat uptake.[44] In the clinic, the use of thermotherapy is conditioned by the presence of pigmented epithelium retinal cells behind the tumor to ensure heat uptake, or otherwise, a pretreatment with intravenous ICG is used to increase thermosensitivity as ICG has an absorption peak at approximately 800 nm (Figure S9).[41] As the tumoroid model does not incorporate pigmented cells, ICG was used here as a thermosensitizer. To define the optimum conditions for the in vitro chemothermotherapy assay, various concentrations of ICG (reported safe dosage of up to 50 μg/mL[45]) and laser power (clinically relevant range between 0.1 and 1.2 W[3]) were tested under irradiation for 5 min. To provide sufficient hyperthermia, the temperature in the well ($T_{base}$) should be higher than 39°C, with the maximum temperature (i.e., temperature of a laser beam spot, $T_{spot}$) not exceeding 60°C, corresponding to subcoagulation temperatures (heatmaps of these two temperatures are shown in Figures 4D and S10).[46] Little or negligible heat uptake was observed at the lowest tested ICG concentration of 5 μg/mL independent of the power applied. Escalation of the ICG concentration and laser power lead to an increase in both $T_{spot}$ and $T_{base}$. Conditions that meet the abovementioned requirements necessitate a compromise involving either higher concentrations of ICG at lower laser powers (e.g. 35–50 μg/mL ICG and 0.3–0.4 W, $T_{spot}$ reaches 59°C and $T_{base}$ reaches 41°C after 5 min of irradiation) or lower concentrations of ICG at higher laser powers (e.g. 10 μg/mL ICG and 0.9–1.0 W, $T_{spot}$ reaches 48°C and $T_{base}$ reaches 39°C after 5 min of irradiation, Figure S10). Interestingly, drug viability assessments revealed that the tumoroids are more sensitive at high ICG concentrations rather than at high laser powers (Figure 4E). Thus, the optimal conditions for our thermotherapy in vitro protocol were defined as 50 μg/mL ICG and 0.3 W of irradiation power.

To validate the model, the efficacy of melphalan and carboplatin, used clinically in chemotherapy and chemothermotherapy, respectively, was assessed (Figures 4F and S6). Melphalan, when used in combination with thermotherapy, did not demonstrate any cytotoxic enhancement in the tumoroid model using ICG and a directed laser (Y79 tumoroid model: $IC_{50}$ values of 163 ± 31 μM at 37°C and 167 ± 78 μM with irradiation for 5 min of 0.3 W and 50 μg/mL ICG; WERI-Rb1 model: 390 ± 169 μM without irradiation and 151 ± 173 μM with irradiation, $T_{spot}$ was 56–59°C, $T_{base}$ was 41–44°C). There was no statistical difference between $IC_{50}$ values in 2D suspension culture as well (Y79 2D: $IC_{50}$ values of 4.4 ± 2.3 μM at 37°C and 4.3 ± 2.5 μM with incubation for 1 h at 42°C; WERI-Rb1 2D: 7.5 ± 6.0 μM at 37°C and 6.5 ± 0.2 μM with incubation for 1 h at 42°C).

Combining carboplatin with 5 min of irradiation of 0.3 W in the presence of 50 μg/mL ICG led to a significant decrease in the $IC_{50}$ value in the Y79 tumoroid model, from 843 ± 75 μM at 37°C to 246 ± 89 μM when combined with focal therapy (Figure 4F). Although not significant, the $IC_{50}$ value decreased with irradiation in WERI-Rb1 tumoroids as well, from 345 ± 77 μM to 210 ± 139 μM (Figure S6). The same trend was observed in the 2D culture with the $IC_{50}$ value significantly decreasing from 62.4 ± 3.5 μM at 37°C to 53.3 ± 1.7 μM at 42°C in Y79 cells and from 22.6 ± 6.0 μM to 0.86 ± 0.03 μM in WERI-Rb1 cells. As a further control, the chemothermotherapy protocol used in 2D culture was tested on the tumoroid model, that is, 1 h incubation at 42°C followed by 71 h at 37°C, which resulted in no cytotoxic enhancement with a TER value of 0.6 and 1.1 for Y79 and WERI-Rb1 tumoroid models, respectively. This observation confirms that the laser-based thermotherapy system provides a chemotherapeutic response close to the clinical experience and enabling putative drugs to be evaluated in combination with thermotherapy.

To investigate whether the enhancement effect of chemothermotherapy is conditioned by a specific structure of carboplatin or by the presence of metal atom, we tested other metal-based drugs – Pt-based cisplatin and Ru-based RAPTA-T on Y79 tumoroid model (Figure S11). We observed that carboplatin has the highest thermal enhancement ratio (3.4) among tested drugs (TER for cisplatin and RAPTA-T is 1.3 and 1.1, respectively). Notably, $IC_{50}$ values of cisplatin were the lowest among all the conditions tested, and even for cisplatin alone, they are comparable with hyperthermia-enhanced carboplatin. Cisplatin was reported to have higher cytotoxicity towards the Y79 cell line in vitro than carboplatin[47] Despite its higher efficacy towards cancer cells, cisplatin is modestly used in pediatric cancers due to its nephro- and ototoxicity.[48]

RAPTA-T was chosen for this experiment due to its previously reported cytotoxicity towards adenocarcinoma and breast cancer cells.[49,50] Compared to cisplatin and carboplatin, RAPTA-T showed the lowest cytotoxic effect, and the lowest TER.

## 4 | DISCUSSION

Three-dimensional cellular models continue to attract interest in drug discovery as they provide a physiologically relevant, self-organizing environment, which resemble tissue and are a better indicator of in vivo activity compared to 2D cultures.[24,51–53] Retinoblastoma 3D models, from simpler spheroids to sophisticated stem cell-derived organoids,[25,26,31,54] were reported to phenotypically and morphologically reproduce retinoblastoma tumors.[31,55] However, to determine whether the tumoroid model reflects clinical observations closer than 2D culture, it is essential to strictly reproduce the clinical treatment mode.[56] Here, we report a robust and reliable tumoroid model, established from two retinoblastoma cell lines, Y79 and WERI-Rb1. Both of these cell lines harbor *RB1* loss, and *MYCN* amplification (Y79) or gain (WERI-Rb1) and are thus representative of most retinoblastoma cases.[57] Nevertheless, the small subset of retinoblastoma tumors (1.4%) harboring *MYCN* amplification and WT *RB1* is not represented by our models and would thus require further investigation.[58,59]

The scaffold-based approach to generate retinoblastoma tumoroids described herein exhibits advantages compared to free-floating spheroids, for example, expanded culture timeline and reproducibility, and allows the implementation of clinically relevant protocols. Repeated intravitreal chemotherapy protocol that is widely implemented for the management of vitreous seeding was adapted to in vitro use in this study. The tumoroid model response to this protocol correlates with clinical observations of vitreous seeding response to the intravitreal chemotherapy.[9,38]

Thermotherapy and chemothermotherapy are often combined and widely implemented in the treatment of retinoblastoma to control small confined tumors, as well as in the treatment of other intraocular cancers, such as ocular melanomas and hemangiomas.[60,61] Although there is no agreement or standard among clinical groups/protocols on chemothermotherapy or randomized clinical trials that could clearly state the benefits of thermotherapy in addition to chemotherapy,[62] it was reported that addition of thermotherapy to chemotherapy resulted in better tumor control at 4-year follow-up (83% compared to 63% in case of chemotherapy alone).[63] Indocyanine green, a clinically used thermosensitizer, after irradiation with near infrared laser converts 85% of energy to heat by internal conversion.[64,65] In this study, an 810 nm diode laser was configured to mimic thermotherapy on the tumoroid model. The chemothermotherapy system was validated with known clinically used agents, and can serve as an accurate indicator of drug activity for chemothermotherapy. Although the use of carboplatin with thermotherapy is mostly empirical, and there is a lack of randomized clinical studies showing therapeutic benefits of such a combination,[62,63] platinum-based drugs were reported to show greater effect in combination with thermotherapy.[66] Heat enhances intracellular platinum accumulation and reduces intracellular detoxification, leading to more platinum-induced DNA adducts and inhibiting their repair.[67] It is not clear why melphalan does not show an enhancement when combined with focal thermotherapy, despite earlier works reporting the treatment benefits of melphalan combined with thermal plaque.[68,69] In our system, we have observed that the combined effect of chemo- and thermotherapy depends on the drug (no universal effect for all metal-based drugs) and on the cytotoxicity level of the chemotherapeutic agent. The high toxicity of melphalan could explain the lack of cytotoxicity enhancement with thermotherapy. This is an important factor to consider, as chemotherapy-associated side-effects are a major burden for young patients with retinoblastoma. Screening more drugs in our system to combine chemo- and thermotherapy would then allow to select molecules with few side-effects and a high efficiency on targeted cancer cell death. With control of temperature, laser power, and thermosensitizer concentration, this versatile system provides a more methodological approach to optimize clinical chemothermotherapy protocols than the current experience-based approach. This new protocol can facilitate the discovery of novel drug candidates to be used in well-established techniques not only for retinoblastoma, but potentially for other intraocular cancers.[61]

In summary, this new tumoroid model has potential to identify new drugs for chemotherapy and chemothermotherapy for the treatment of retinoblastoma. Further development implies model adaptation for other cancers, where metronomic and laser-based therapies (e.g., photodynamic therapy) are relevant.[70–72] Finally, the model is beneficial in the development of heat-activated drug formulations to be used for chemothermotherapy.[73-75]

## AUTHOR CONTRIBUTIONS

Conceptualization: PJD. Formal analysis: FK, ILS, Methodology: AB, FK, ILS. Investigation: ILS, VS, PA, AM. Visualization: ILS. Resources: PJD, FLM. Supervision: PJD, FLM, AB. Writing – original draft: ILS. Writing – review and editing: all authors.

## ACKNOWLEDGMENTS

We thank Mrs. Elea Lalys for assistance in immunohistochemistry experiments, Mr. Quentin Gasser for assistance in 2D cytotoxicity experiments, the EPFL BioImaging and Optics Core Facility, particularly Dr. Nicolas Chiaruttini, for assistance in imaging, and the EPFL Biomolecular Screening Facility, particularly Mr. Julien Bortoli, for assistance in drug preparation.

## FUNDING INFORMATION

This project received funding from the European Union's Horizon 2020 research and innovation program under the Marie Skłodowska-Curie grant agreement no. 754354 (ILS).

## CONFLICT OF INTEREST STATEMENT

The authors declare no conflict of interest.

## ETHICS STATEMENT

Approval of the research protocol by an institutional review board: N/A.

Informed consent: N/A.

Registry and the registration no. of the study/trial: N/A.

Animal studies: N/A.

## ORCID

*Irina L. Sinenko* https://orcid.org/0000-0002-9172-835X
*Fabien Kuttler* https://orcid.org/0000-0003-2575-1989
*Adeline Berger* https://orcid.org/0000-0003-2986-4489

## REFERENCES

1. Kivelä T. The epidemiological challenge of the most frequent eye cancer: retinoblastoma, an issue of birth and death. *Br J Ophthalmol*. 2009;93(9):1129-1131. doi:10.1136/bjo.2008.150292
2. Fernandes AG, Pollock BD, Rabito FA. Retinoblastoma in the United States: a 40-year incidence and survival analysis. *J Pediatr Ophthalmol Strabismus*. 2018;55(3):182-188. doi:10.3928/01913913-20171116-03
3. Munier FL, Beck-Popovic M, Chantada GL, et al. Conservative management of retinoblastoma: challenging orthodoxy without compromising the state of metastatic grace. "Alive, with good vision and no comorbidity.". *Prog Retin Eye Res*. 2019;73:100764. doi:10.1016/j.preteyeres.2019.05.005

4. Xu XL, Singh HP, Wang L, et al. Rb suppresses human cone-precursor-derived retinoblastoma tumours. *Nature*. 2014;514(7522):385-388. doi:10.1038/nature13813
5. Munier FL. Classification and management of seeds in retinoblastoma. *Ophthalmic Genet*. 2014;35(4):193-207. doi:10.3109/13816810.2014.973045
6. Fabian ID, Reddy A, Sagoo MS. Classification and staging of retinoblastoma. *Community Eye Health*. 2018;31(101):11-13.
7. Mendoza PR, Grossniklaus HE. Therapeutic options for retinoblastoma. *Cancer Control*. 2016;23(2):99-109. doi:10.1177/107327481602300203
8. Shields CL, Kaliki S, Al-Dahmash S, et al. Management of advanced retinoblastoma with intravenous chemotherapy then intra-arterial chemotherapy as alternative to enucleation. *Retina*. 2013;33(10):2103-2109. doi:10.1097/IAE.0b013e318295f783
9. Munier FL, Gaillard MC, Balmer A, et al. Intravitreal chemotherapy for vitreous disease in retinoblastoma revisited: from prohibition to conditional indications. *Br J Ophthalmol*. 2012;96(8):1078-1083. doi:10.1136/bjophthalmol-2011-301450
10. Munier FL, Moulin A, Gaillard MC, et al. Intracameral chemotherapy for globe salvage in retinoblastoma with secondary anterior chamber invasion. *Ophthalmology*. 2018;125(4):615-617. doi:10.1016/j.ophtha.2017.11.010
11. Abramson DH, Schefler AC. Transpupillary thermotherapy as initial treatment for small intraocular retinoblastoma: technique and predictors of success. *Ophthalmology*. 2004;111(5):984-991. doi:10.1016/j.ophtha.2003.08.035
12. Lumbroso L, Doz F, Urbieta M, et al. Chemothermotherapy in the management of retinoblastoma. *Ophthalmology*. 2002;109(6):1130-1136. doi:10.1016/S0161-6420(02)01053-9
13. Murphree AL, Judith G, Malogolowkin M, Parker R, Reed E, Gomer CJ. Chemotherapy plus local treatment in the management of intraocular retinoblastoma. *Arch Ophthalmol*. 1996;114:1348-1356.
14. Chan HSL, Gallie BL, Munier FL, Popovic MB. Chemotherapy for retinoblastoma. *Ophthalmol Clin North Am*. 2005;18(1):55-63. doi:10.1016/j.ohc.2004.11.002
15. Schaiquevich P, Fabius AW, Francis JH, Chantada GL, Abramson DH. Ocular pharmacology of chemotherapy for retinoblastoma. *Retina*. 2017;37(1):1-10. doi:10.1097/IAE.0000000000001275
16. Reid TW, Albert DM, Rabson AS, et al. Characteristics of an established cell line of retinoblastoma. *J Natl Cancer Inst*. 1974;53(2):347-360. doi:10.1093/jnci/53.2.347
17. McFall RC, Sery TW, Makadon M. Characterization of a new continuous cell line derived from a human retinoblastoma. *Cancer Res*. 1977;37(4):1003-1010.
18. Windle JJ, Albert DM, O'Brien JM, et al. Retinoblastoma in transgenic mice. *Nature*. 1990;343(6259):665-669. doi:10.1038/343665a0
19. Pascual-Pasto G, Olaciregui NG, Vila-Ubach M, et al. Preclinical platform of retinoblastoma xenografts recapitulating human disease and molecular markers of dissemination. *Cancer Lett*. 2016;380(1):10-19. doi:10.1016/j.canlet.2016.06.012
20. Sinenko IL, Turnell-Ritson RC, Munier FL, Dyson PJ. The predictive capacity of in vitro preclinical models to evaluate drugs for the treatment of retinoblastoma. *Exp Eye Res*. 2023;230:109447. doi:10.1016/j.exer.2023.109447
21. Benavente CA, McEvoy JD, Finkelstein D, et al. Cross-species genomic and epigenomic landscape of retinoblastoma. *Oncotarget*. 2013;4(6):844-859. doi:10.18632/oncotarget.1051
22. Nair RM, Kaliki S, Vemuganti GK. Animal models in retinoblastoma research. *Saudi J Ophthalmol*. 2013;27(3):141-146. doi:10.1016/j.sjopt.2013.06.008
23. Brennan RC, Federico S, Bradley C, et al. Targeting the p53 pathway in retinoblastoma with subconjunctival nutlin-3a. *Cancer Res*. 2011;71(12):4205-4213. doi:10.1158/0008-5472.CAN-11-0058
24. Langhans SA. Three-dimensional in vitro cell culture models in drug discovery and drug repositioning. *Front Pharmacol*. 2018;9:1-14. doi:10.3389/fphar.2018.00006
25. Norrie JL, Nityanandam A, Lai K, et al. Retinoblastoma from human stem cell-derived retinal organoids. *Nat Commun*. 2021;12(1):4535. doi:10.1038/s41467-021-24781-7
26. Bond WS, Akinfenwa PY, Perlaky L, Hurwitz MY, Hurwitz RL, Chévez-Barrios P. Tumorspheres but not adherent cells derived from retinoblastoma tumors are of malignant origin. *PLoS One*. 2013;8(6):4-10. doi:10.1371/journal.pone.0063519
27. Saengwimol D, Rojanaporn D, Chaitankar V, et al. A three-dimensional organoid model recapitulates tumorigenic aspects and drug responses of advanced human retinoblastoma. *Sci Rep*. 2018;8(1):1-13. doi:10.1038/s41598-018-34037-y
28. Bishop PN. Structural macromolecules and supramolecular organisation of the vitreous gel. *Prog Retin Eye Res*. 2000;19(3):323-344.
29. Donati S, Caprani SM, Airaghi G, et al. Vitreous substitutes: the present and the future. *Biomed Res Int*. 2014;2014:1-12. doi:10.1155/2014/351804
30. Stringer C, Wang T, Michaelos M, Pachitariu M. Cellpose: a generalist algorithm for cellular segmentation. *Nat Methods*. 2021;18(1):100-106. doi:10.1038/s41592-020-01018-x
31. Winter U, Aschero R, Fuentes F, et al. Tridimensional retinoblastoma cultures as vitreous seeds models for live-cell imaging of chemotherapy penetration. *Int J Mol Sci*. 2019;20(5):1077. doi:10.3390/ijms20051077
32. Tang Z, Ma H, Mao Y, et al. Identification of stemness in primary retinoblastoma cells by analysis of stem-cell phenotypes and tumorigenicity with culture and xenograft models. *Exp Cell Res*. 2019;379(1):110-118. doi:10.1016/j.yexcr.2019.03.034
33. Vuhahula EA, Jumanne S, Yahaya J. Expression of Ki67 as detected by MIB-1 and its association with histopathological high-risk factors among patients with retinoblastoma tumour: a cross-sectional study. *BMJ Open Ophthalmol*. 2022;7(1):e000984. doi:10.1136/bmjophth-2022-000984
34. Liu J, Ottaviani D, Sefta M, et al. A high-risk retinoblastoma subtype with stemness features, dedifferentiated cone states and neuronal/ganglion cell gene expression. *Nat Commun*. 2021;12:5578. doi:10.1038/s41467-021-25792-0
35. Zhang JH, Chung TDY, Oldenburg KR. A simple statistical parameter for use in evaluation and validation of high throughput screening assays. *J Biomol Screen*. 1999;4(2):67-73. doi:10.1177/108705719900400206
36. Mitra M, Mohanty C, Harilal A, Maheswari UK, Sahoo SK, Krishnakumar S. A novel in vitro three-dimensional retinoblastoma model for evaluating chemotherapeutic drugs. *Mol Vis*. 2012;18:1361-1378.
37. Friedrich J, Seidel C, Ebner R, Kunz-Schughart LA. Spheroid-based drug screen: considerations and practical approach. *Nat Protoc*. 2009;4(3):309-324. doi:10.1038/nprot.2008.226
38. Francis JH, Abramson DH, Gaillard MC, Marr BP, Beck-Popovic M, Munier FL. The classification of vitreous seeds in retinoblastoma and response to intravitreal melphalan. *Ophthalmology*. 2015;122(6):1173-1179. doi:10.1016/j.ophtha.2015.01.017
39. Abramson DH, Frank CM, Chantada GL, et al. Intraocular carboplatin concentrations following intravenous administration for human intraocular retinoblastoma. *Ophthalmic Genet*. 1999;20(1):31-36. doi:10.1076/opge.20.1.31.2302
40. Smith DW, Lee CJ, Gardiner BS. No flow through the vitreous humor: how strong is the evidence? *Prog Retin Eye Res*. 2020;78:100845. doi:10.1016/j.preteyeres.2020.100845
41. Francis JH, Abramson DH, Brodie SE, Marr BP. Indocyanine green enhanced transpupillary thermotherapy in combination with ophthalmic artery chemosurgery for retinoblastoma. *Br J Ophthalmol*. 2013;97(2):164-168. doi:10.1136/bjophthalmol-2012-302495
42. Clavel CM, Zava O, Schmitt F, et al. Thermoresponsive chlorambucil derivatives for tumour targeting. *Angew Chem Int Ed*. 2011;50(31):7124-7127. doi:10.1002/anie.201101133
43. Renfrew AK, Scopelliti R, Dyson PJ. Use of perfluorinated phosphines to provide thermomorphic anticancer complexes for

heat-based tumor targeting. *Inorg Chem*. 2010;49(5):2239-2246. doi:10.1021/IC9020433/SUPPL_FILE/IC9020433_SI_001.CIF
44. Soliman S, Kletke S, Roelofs K, VandenHoven C, Mckeen L, Gallie B. Precision laser therapy for retinoblastoma. *Expert Rev Ophthalmol*. 2018;13(3):149-159. doi:10.1080/17469899.2018.1478729
45. Stanescu-Segall D, Jackson TL. Vital staining with indocyanine green: a review of the clinical and experimental studies relating to safety. *Eye*. 2009;23(3):504-518. doi:10.1038/eye.2008.249
46. Dithmar S. Transpupillary thermotherapy. *Age-Related Macular Degeneration*. Springer; 2004:159-167. doi:10.1007/978-3-662-05199-3_11
47. Di Felice V, Lauricella M, Giuliano M, Emanuele S, Vento R, Tesoriere G. The apoptotic effects of cisplatin and carboplatin in retinoblastoma Y79 cells. *Int J Oncol*. 1998;13(2):225-232. doi:10.3892/ijo.13.2.225
48. Ruggiero A, Trombatore G, Triarico S, et al. Platinum compounds in children with cancer: toxicity and clinical management. *Anticancer Drugs*. 2013;24(10):1007-1019. doi:10.1097/CAD.0b013e3283650bda
49. Scolaro C, Bergamo A, Brescacin L, et al. In vitro and in vivo evaluation of ruthenium(II)-arene PTA complexes. *J Med Chem*. 2005;48(12):4161-4171. doi:10.1021/jm050015d
50. Nhukeaw T, Hongthong K, Dyson PJ, Ratanaphan A. Cellular responses of BRCA1-defective HCC1937 breast cancer cells induced by the antimetastasis ruthenium(II) arene compound RAPTA-T. *Apoptosis*. 2019;24(7–8):612-622. doi:10.1007/S10495-019-01544-W/FIGURES/8
51. Langhans SA. Using 3D in vitro cell culture models in anti-cancer drug discovery. *Expert Opin Drug Discovery*. 2021;16(8):841-850. doi:10.1080/17460441.2021.1912731
52. Drost J, Clevers H. Organoids in cancer research. *Nat Rev Cancer*. 2018;18(7):407-418. doi:10.1038/s41568-018-0007-6
53. Broutier L, Mastrogiovanni G, Verstegen MMA, et al. Human primary liver cancer-derived organoid cultures for disease modeling and drug screening. *Nat Med*. 2017;23(12):1424-1435. doi:10.1038/nm.4438
54. Liu H, Zhang Y, Zhang Y-Y, et al. Human embryonic stem cell-derived organoid retinoblastoma reveals a cancerous origin. *Proc Natl Acad Sci U S A*. 2020;117(52):33628-33638. doi:10.1073/pnas.2011780117
55. Pascual-Pasto G, Bazan-Peregrino M, Olaciregui NG, et al. Therapeutic targeting of the RB1 pathway in retinoblastoma with the oncolytic adenovirus VCN-01. *Sci Transl Med*. 2019;11(476):1-12. doi:10.1126/scitranslmed.aat9321
56. Cancela MB, Zugbi S, Winter U, et al. A decision process for drug discovery in retinoblastoma. *Invest New Drugs*. 2020;39(2):426-441. doi:10.1007/S10637-020-01030-0
57. Schwermer M, Hiber M, Dreesmann S, et al. Comprehensive characterization of RB1 mutant and MYCN amplified retinoblastoma cell lines. *Exp Cell Res*. 2019;375(2):92-99. doi:10.1016/j.yexcr.2018.12.018
58. Roohollahi K, de Jong Y, van Mil SE, Fabius AWM, Moll AC, Dorsman JC. High-level MYCN-amplified RB1-proficient retinoblastoma tumors retain distinct molecular signatures. *Ophthalmol Sci*. 2022;2(3):100188. doi:10.1016/J.XOPS.2022.100188
59. Zugbi S, Ganiewich D, Bhattacharyya A, et al. Clinical, genomic, and pharmacological study of MYCN-amplified RB1 wild-type metastatic retinoblastoma. *Cancer*. 2020;12(9):1-20. doi:10.3390/cancers12092714
60. Journée-De Korver JG, Keunen JEE. Thermotherapy in the management of choroidal melanoma. *Prog Retin Eye Res*. 2002;21(3):303-317. doi:10.1016/S1350-9462(02)00005-8
61. Houston SK, Wykoff CC, Berrocal AM, Hess DJ, Murray TG. Lasers for the treatment of intraocular tumors. *Lasers Med Sci*. 2013;28(3):1025-1034. doi:10.1007/s10103-012-1052-0
62. Fabian ID, Johnson KP, Stacey AW, Sagoo MS, Reddy MA. Focal laser treatment in addition to chemotherapy for retinoblastoma. *Cochrane Database Syst Rev*. 2017;2017(6):CD012366. doi:10.1002/14651858.CD012366.pub2
63. Shields CL. Macular retinoblastoma managed with Chemoreduction. *Arch Ophthalmol*. 2005;123(6):765-773. doi:10.1001/archopht.123.6.765
64. Shafirstein G, Bäumler W, Hennings LJ, et al. Indocyanine green enhanced near-infrared laser treatment of murine mammary carcinoma. *Int J Cancer*. 2012;130(5):1208-1215. doi:10.1002/ijc.26126
65. Li J, Zhang W, Ji W, et al. Near infrared photothermal conversion materials: mechanism, preparation, and photothermal cancer therapy applications. *J Mater Chem B*. 2021;9(38):7909-7926. doi:10.1039/d1tb01310f
66. Kampinga HH. Cell biological effects of hyperthermia alone or combined with radiation or drugs: a short introduction to newcomers in the field. *Int J Hyperthermia*. 2006;22:191-196. doi:10.1080/02656730500532028
67. Hettinga JVE, Konings AWT, Kampinga HH. Reduction of cellular cisplatin resistance by hyperthermia—a reviews. *Int J Hyperthermia*. 2009;13(5):439-457. doi:10.3109/02656739709023545
68. Inomata M, Kaneko A, Kunimoto T, Saijo N. In vitro thermo- and thermochemo-sensitivity of retinoblastoma cells from surgical specimens. *Int J Hyperthermia*. 2002;18(1):50-61. doi:10.1080/02656730110087068
69. Kaneko A. Japanese contributions to ocular oncology. *Int J Clin Oncol*. 1999;4(6):321-326. doi:10.1007/s101470050078
70. Cazzaniga ME, Cordani N, Capici S, Cogliati V, Riva F, Cerrito MG. Metronomic chemotherapy. *Cancer*. 2021;13(9):1-27. doi:10.3390/cancers13092236
71. Broekgaarden M, Bulin AL, Frederick J, Mai Z, Hasan T. Tracking photodynamic- and chemotherapy-induced redox-state perturbations in 3D culture models of pancreatic cancer: a tool for identifying therapy-induced metabolic changes. *J Clin Med*. 2019;8(9):1399. doi:10.3390/jcm8091399
72. Nasr S, Rady M, Sebak A, et al. A naturally derived carrier for photodynamic treatment of squamous cell carcinoma: In vitro and in vivo models. *Pharmaceutics*. 2020;12(6):494. doi:10.3390/pharmaceutics12060494
73. Clavel CM, Nowak-Sliwinska P, Pəunescu E, Dyson PJ. Thermoresponsive fluorinated small-molecule drugs: a new concept for efficient localized chemotherapy. *MedChemComm*. 2015;6(12):2054-2062. doi:10.1039/c5md00409h
74. Amin M, Huang W, Seynhaeve ALB, Ten Hagen TLM. Hyperthermia and temperature-sensitive nanomaterials for spatiotemporal drug delivery to solid tumors. *Pharmaceutics*. 2020;12(11):1-23. doi:10.3390/pharmaceutics12111007
75. Dunne M, Epp-Ducharme B, Sofias AM, Regenold M, Dubins DN, Allen C. Heat-activated drug delivery increases tumor accumulation of synergistic chemotherapies. *J Control Release*. 2019;308:197-208. doi:10.1016/j.jconrel.2019.06.012

## SUPPORTING INFORMATION

Additional supporting information can be found online in the Supporting Information section at the end of this article.

**How to cite this article:** Sinenko IL, Kuttler F, Simeonov V, et al. Translational screening platform to evaluate chemotherapy in combination with focal therapy for retinoblastoma. *Cancer Sci*. 2023;114:3728-3739. doi:10.1111/cas.15878